Synthesis of Porous Carbon Supported Palladium Nanoparticle Catalysts by Atomic Layer Deposition: Application for Rechargeable Lithium−O$_2$ Battery

Yu Lei,[†,∇] Jun Lu,[‡,∇] Xiangyi Luo,[‡,∥,∇] Tianpin Wu,[§] Peng Du,[‡] Xiaoyi Zhang,[§] Yang Ren,[§] Jianguo Wen,[⊥] Dean J. Miller,[⊥] Jeffrey T. Miller,[‡] Yang-Kook Sun,[#] Jeffrey W. Elam,*[,†] and Khalil Amine*[,‡,○]

[†]Energy Systems Division, Argonne National Laboratory, Argonne, Illinois 60439, United States

[‡]Chemical Science and Engineering Division, Argonne National Laboratory, Argonne, Illinois 60439, United States

[§]X-ray Science Division, Advanced Photon Sources, Argonne National Laboratory, Argonne, Illinois 60439, United States

[∥]Department of Metallurgical Engineering, University of Utah, Salt Lake City, Utah 84112, United States

[⊥]Electron Microscopy Center, Argonne National Laboratory, Argonne, Illinois 60439, United States
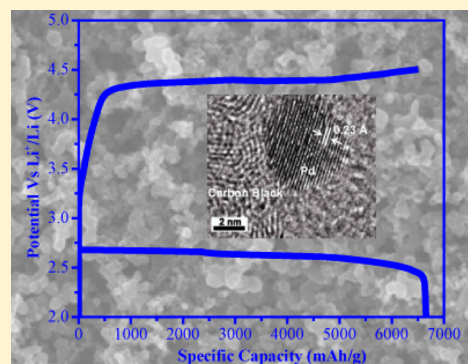
[#]Department of Energy Engineering, Hanyang University, Seoul 133-791, South Korea

[○]Faculty of Science, Chemistry Department, King Abdulaziz University, 80203 Jeddah, Saudi Arabia

S *Supporting Information*

ABSTRACT: In this study, atomic layer deposition (ALD) was used to deposit nanostructured palladium on porous carbon as the cathode material for Li−O$_2$ cells. Scanning transmission electron microscopy showed discrete crystalline nanoparticles decorating the surface of the porous carbon support, where the size could be controlled in the range of 2−8 nm and depended on the number of Pd ALD cycles performed. X-ray absorption spectroscopy at the Pd K-edge revealed that the carbon supported Pd existed in a mixed phase of metallic palladium and palladium oxide. The conformality of ALD allowed us to uniformly disperse the Pd catalyst onto the carbon support while preserving the initial porous structure. As a result, the charging and discharging performance of the oxygen cathode in a Li−O$_2$ cell was improved. Our results suggest that ALD is a promising technique for tailoring the surface composition and structure of nanoporous supports in energy storage devices.

KEYWORDS: *Li−O$_2$ battery, atomic layer deposition, palladium nanoparticles, oxygen reduction reaction, oxygen evolution reaction*

The Li−O$_2$ battery is currently the subject of intense scientific investigation due to the extremely high theoretical energy density of 12 kWh/kg, which far exceeds that of any other existing energy storage technology.[1−22] The tremendous theoretical energy density results from using lithium metal as the anode, and from utilizing ambient oxygen as the cathode oxidant, eliminating the need for an on-board oxygen source and the associated weight penalty. In the Li−O$_2$ battery, the oxygen electrode should be porous to store the solid products generated from the reaction of Li ions with O$_2$ during the discharge, and it must integrate a catalyst to promote this reaction. It has been found that a variety of factors dictate the extent of electrochemical (discharge and charge) reactions in Li−O$_2$ cells including the nature of the catalyst, the catalyst distribution on the porous cathode, the pore volume of the cathode, as well as the type of the applied organic electrolytes.[6,16,17,23−25] The design of the oxygen electrode is therefore critical to realizing the full potential of the Li−O$_2$ cell.[6]

Both the surface area and porosity of the cathode are critical for the performance of lithium−O$_2$ batteries. Larger surface areas provi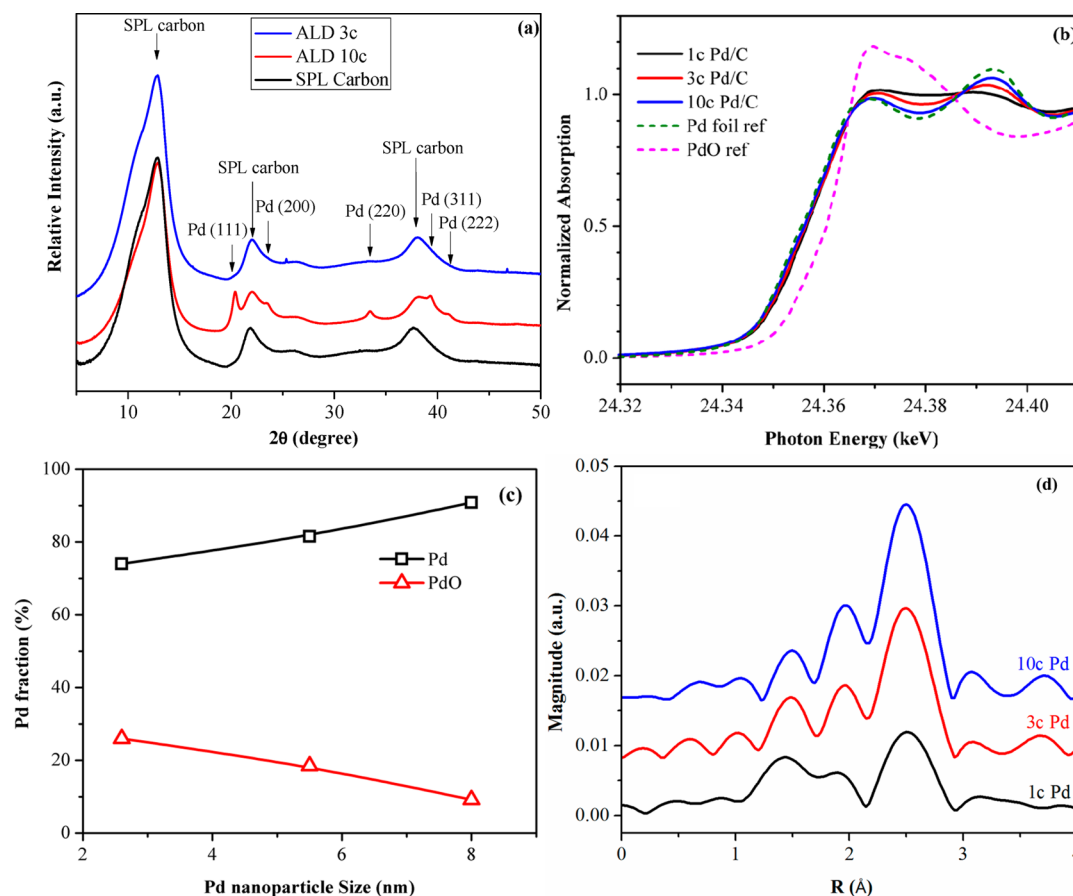de more catalyst particles and catalytically active sites to accelerate the electrochemical reactions. However, larger surface areas do not always yield larger specific capacities, as has been shown in a previous study by Kuboki et al.[26] In our recent work on MnO$_2$ catalysts for Li−O$_2$ batteries, we also demonstrated the effects of the cathode porosity on the electrochemical performance, especially the cyclability of the cell, by controlled experiments.[27] These results illustrate the importance of porosity and, in particular, the pore size. Larger pores facilitate faster oxygen diffusion and provide the volume necessary to accommodate the reduction products deposited during discharge.

For practical applications, the Li−O$_2$ battery must be rechargeable and these necessitates using a sufficiently high potential or a catalyst to promote the electrochemical reactions.[1,4] However, high overpotentials on charge and discharge, even at very low current densities of 0.01−0.05

Figure 1. (a) High-resolution XRD patterns of original SPL carbon and SPL carbon after being loaded with Pd catalyst using 3 and 10 cycles of Pd ALD. (b) XANES spectra for 1c Pd (black solid line), 3c Pd (red solid line), 10c Pd (blue solid line), and XANES reference spectra for metallic Pd foil reference (olive dashed line) and Pd oxide reference (magenta dashed line). (c) Pd oxide fraction of Pd/C samples, obtained using XANES linear combination. (d) Fourier transform of X-ray absorption spectra (k^2: Δk = 2.8−11 Å^{-1}). Fitting this data provides the data in Table 1.

mA/cm^2, result in very low round-trip efficiencies (<60%) and low power capability. It is strongly believed to be dependent on the nature of catalysts applied and their loading process onto the high-surface-area cathode. Metals, metal complexes, and metal oxides have all been examined as the cathode catalysts in the Li−O$_2$ cells, and these catalysts show large differences in discharge capacity and charge plateau.[1,2,14−17,19,28−32] However, it should be pointed out that in most of the cases these catalysts are presynthesized and then dispersed onto the carbon support by mechanical milling.[16,23,24,33] This process can destroy the porous structure of carbon, and is unable to distribute the catalysts on the carbon support uniformly, both of which might severely affect the charge/discharge properties of the oxygen cathode. Consequently, a method is needed for dispersing catalysts with well-controlled particle size uniformly onto the carbon support.

Atomic layer deposition (ALD) is a technique for preparing thin films on planar substrates that employs self-limiting chemical reactions between gaseous precursors and a solid surface allowing atomic scale control over the film thickness and composition.[34,35] One of the distinguishing attributes of ALD is the capability to deposit highly uniform and conformal coatings on surfaces with complex topographies and to infiltrate mesoporous materials.[36−38] This feature is particularly attractive for the synthesis of heterogeneous catalysts requiring highly dispersed catalytic species on high surface area,

mesoporous supports. Consequently, ALD is being explored as an alternative method for preparing advanced catalysts.[39−43]
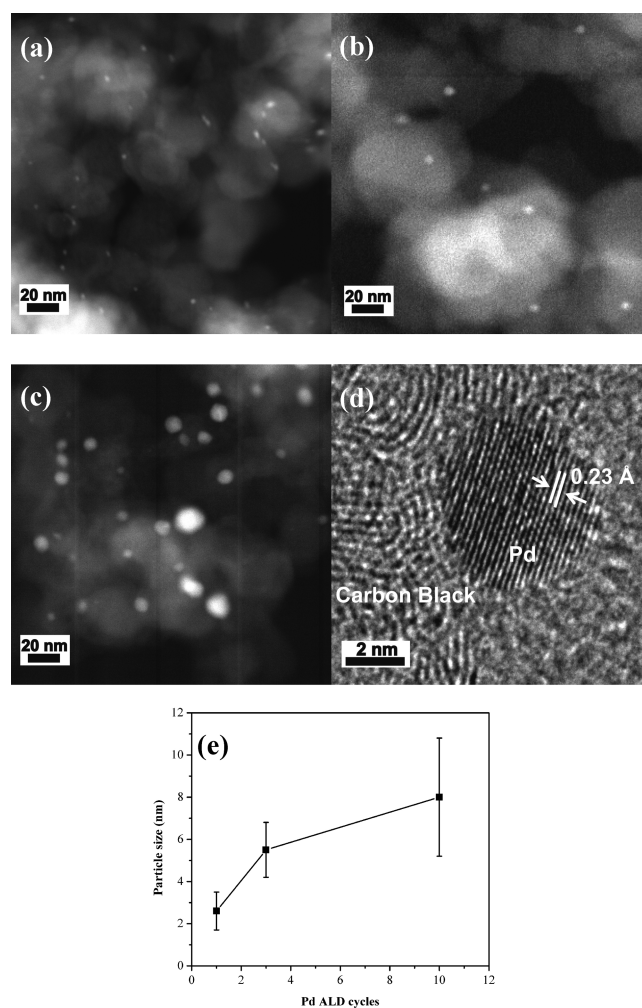
The layer-by-layer growth process afforded by ALD typically yields smooth, uniform films, and this is ideal for most microelectronics applications. However, nonuniform deposits can occur when the ALD chemistry is inhibited on the starting substrate or when the ALD material aggregates from surface diffusion. Both of these mechanisms are in effect in the early stages of noble metal ALD on oxide surfaces, which result in the formation of discrete, three-dimensional nanoparticles decorating the surface. This behavior has been exploited to synthesize supported noble metal catalysts exhibiting remarkably high activity as a result of the highly dispersed, small noble metal particles.[44−47] The good dispersion of the active particles on the support during ALD enables a decrease of the metal loading while still achieving the same catalytic activity as the catalysts with higher metal loading prepared by other methods. This is especially important with noble metal materials where the excess use of the raw materials should be avoided. Uniform palladium nanoparticles in the size range from subnanometer to a few nanometers, one of the most efficient catalysts for facilitating the oxygen reduction reaction (ORR) in the fuel cell, have been synthesized by ALD on high surface area supports.[44,45,48,49] However, performing ALD on a porous carbon surface in general has been a technical challenge because of the lack of active sites on carbon for surface reactions, and therefore has not been well studied.

In this study, we demonstrate that uniformly dispersed Pd nanoparticles onto a porous carbon support prepared by the ALD process exhibit high electrochemical catalytic activity in a Li−O$_2$ cell for the first time. Scanning transmission electron microscopy (STEM) and X-ray absorption spectroscopy (XAS) are used to characterize the structure and composition of the ALD Pd/C electrocatalysts. The electrochemical activity of these catalysts is determined using Swagelok-type Li−O$_2$ cells, and results are compared with those obtained with a bare porous carbon cathode.

The phase purity and crystal structure of the as-prepared ALD Pd/C samples were characterized by high-energy X-ray diffraction (XRD), and the results for the 3-cycle and 10-cycle samples are presented in Figure 1a along with the XRD pattern for the original super P Li (SPL) carbon for comparison. With the exception of the SPL carbon peaks, all the peaks for the 10-cycle ALD Pd/C sample in Figure 1a can be readily indexed to a pure fcc structure with the lattice constant $a = 3.89$ Å, in good agreement with the reported value for Pd found in the inorganic crystal structure database (ICSD). The average grain size for the 10-cycle ALD Pd/C sample is estimated by the Scherrer equation to be ∼7 nm, which is further confirmed by the TEM analysis described below. It was difficult to identify Pd in the 1-cycle and 3-cycle ALD Pd/C samples using XRD due to the relatively low Pd loading. However, Pd in 1-cycle and 3-cycle ALD Pd/C samples can be readily detected using TEM and EXAFS, as demonstrated below.

Representative STEM images of the 1-cycle, 3-cycle, and 10-cycle ALD Pd/C samples are illustrated in Figure 2a−c, respectively. Well-dispersed and uniform Pd nanoparticles were prepared over the SPL carbon after 1 cycle and 3 cycles of Pd ALD. However, the 10-cycle sample shows agglomerated Pd nanoparticles (Figure 2c). The average size of Pd nanoparticles was determined from multiple images recorded for each sample to be 2.6, 5.5, and 8 nm following 1, 3 and 10 ALD cycles of Pd, respectively, as shown in Figure 2e. In comparison to published literature, the average sizes of Pd nanoparticles on the porous carbon are larger than those on metal oxide surfaces prepared using similar conditions. For instance, on alumina (Al$_2$O$_3$), 1 ALD cycle of Pd at 200 °C yields Pd nanoparticles with a diameter of ∼1 nm.[44,50] Only after 25 ALD cycles of Pd does the nanoparticle size increase to 2.9 ± 0.9 nm.[50] Moreover, the metal oxide surfaces yield a higher density of Pd nanoparticles compared to the SPL carbon. These results suggest that there are fewer nucleation sites for the Pd ALD on the SPL carbon as compared to metal oxides, and that Pd diffuses more rapidly on the carbon, yielding a smaller number of larger particles. Nevertheless, the Pd coverage on the carbon surface is very uniform, as supported by the SEM EDX mapping images (Supporting Information, Figure S1). Figure 2d shows a high-resolution transmission electron microscopy (TEM) image for a ∼5.5 nm Pd/C sample, where lattice fringes for the metal nanoparticles are clearly visible. The nanoparticles show lattice fringes of ∼0.23 nm, which is consistent with the *d*-spacing for the Pd [111] plane.[51] These TEM images provide direct evidence that the metal nanoparticles are well crystalline and faceted. In addition, SEM images (Supporting Information, Figure S2) on the samples before and after Pd ALD reveal that the porous structure of the carbon is well preserved during the Pd ALD, which is critical to achieve high performance in Li−O$_2$ cells.

The chemical composition of the Pd nanoparticles was determined using linear combination fitting of X-ray absorption

Figure 2. STEM images of (a) 1c Pd/C, (b) 3c Pd/C, and (c) 10c Pd/C. (d) HRTEM of a Pd nanoparticle ∼5.5 nm in diameter prepared by ALD supported over carbon. (e) Pd particle size as a function of ALD cycles.

near edge structure (XANES) spectra recorded in air at room temperature. To facilitate these measurements, XANES reference spectra were recorded for a Pd foil and a PdO standard, as shown in Figure 1b. The XANES spectra of 1c, 3c, and 10c Pd/C were compared in Figure 1b. With increasing ALD cycles, Pd step edges show a slight shift to lower energy and decreasing whiteline intensity. In comparison to the XANES reference of Pd foil and PdO, this indicates an increase in the percentage of the metallic component for the Pd nanoparticles. The quantitative results obtained from linear combination fittings are illustrated in Figure 1c. The 1-cycle Pd/C with the smallest Pd particle size of ∼2.5 nm consists of ∼26% (atomic percent) PdO, and this is the highest PdO content of the three samples. With increasing particle size, the PdO content decreases linearly to a value of ∼9% for the 8 nm particles. The fraction of surface atoms in these Pd nanoparticles, given by 0.9/size (nm), is 0.36, 0.16, and 0.11 for 2.5, 5.5, and 8 nm Pd and very similar to the fraction of PdO determined from the XANES, suggesting that primarily the surfaces of the Pd particles are oxidized.

Figure 1d shows the Fourier transforms of the extended X-ray absorption fine structure (EXAFS). The peaks at about 2 and 2.5 Å are fingerprint peaks in the first shell for metallic Pd.

The Fourier transform measurements for the ALD Pd samples all show similar features in the first shell, but the peak intensities increase with increasing ALD cycles, i.e., particle size, determined by STEM. In comparison to the Pd foil spectrum, the as-prepared 1-cycle ALD Pd/C measured in air is clearly partially oxidized, showing an additional peak at around 1.4 Å that is typically associated with the Pd−O bond. The EXAFS data were fit, and the results of this quantitative analysis are listed in Table 1. The nearest Pd−Pd bond distances are in

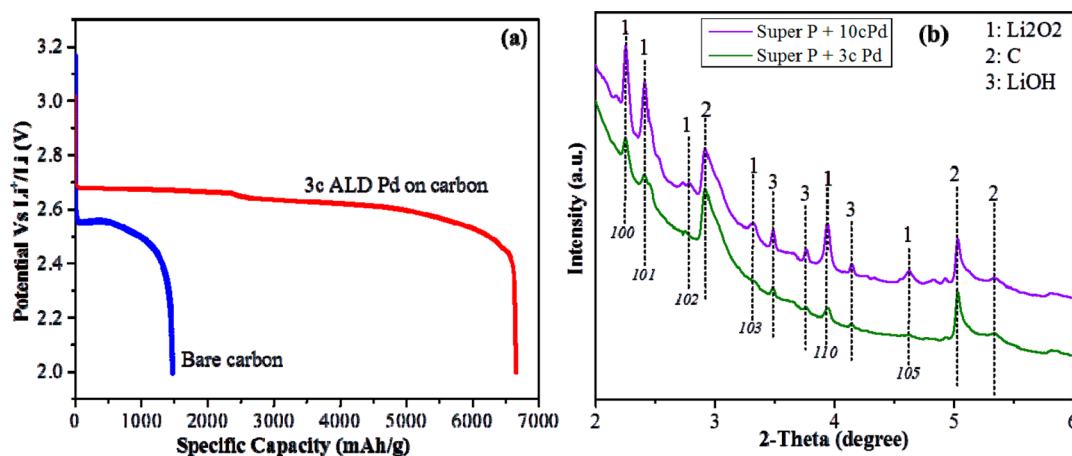**Table 1. Structural Parameters of Different Pd Samples Measured under Ambient Conditions**

sample	TEM size (nm)	scatter	CN	R (Å)	DWF ($\times 10^3$)	E_o (eV)
1c Pd/C	2.6	Pd−Pd	5.3	2.74	3	0.8
		Pd−O	1.3	2.05	1	3.1
3c Pd/C	5.5	Pd−Pd	8.2	2.75	2	0.6
		Pd−O	0.7	2.05	1	2.0
10c Pd/C	8	Pd−Pd	9.2	2.74	1	1.4
		Pd−O	0.4	2.05	1	3.8

good agreement with XRD data (2.76 Å). As expected, the Pd−Pd coordination number increases with increasing particle size. The coordination number of nearest Pd−O neighbors in the Pd oxide reference is 4. Thus, the percentage of PdO in the ALD Pd/C samples can also be calculated as $CN_{Pd−O}/4$. The fractions of PdO calculated from the EXAFS measurements are 32.5, 17.5, and 10% for the 1c, 3c, and 10c ALD Pd/C samples, respectively, which are within the error of the results obtained from the XANES linear combination fittings. Similar to the XANES analysis, the fraction of the oxidized Pd determined from the EXAFS fits is very similar to the fraction of surface Pd in these metallic nanoparticles.
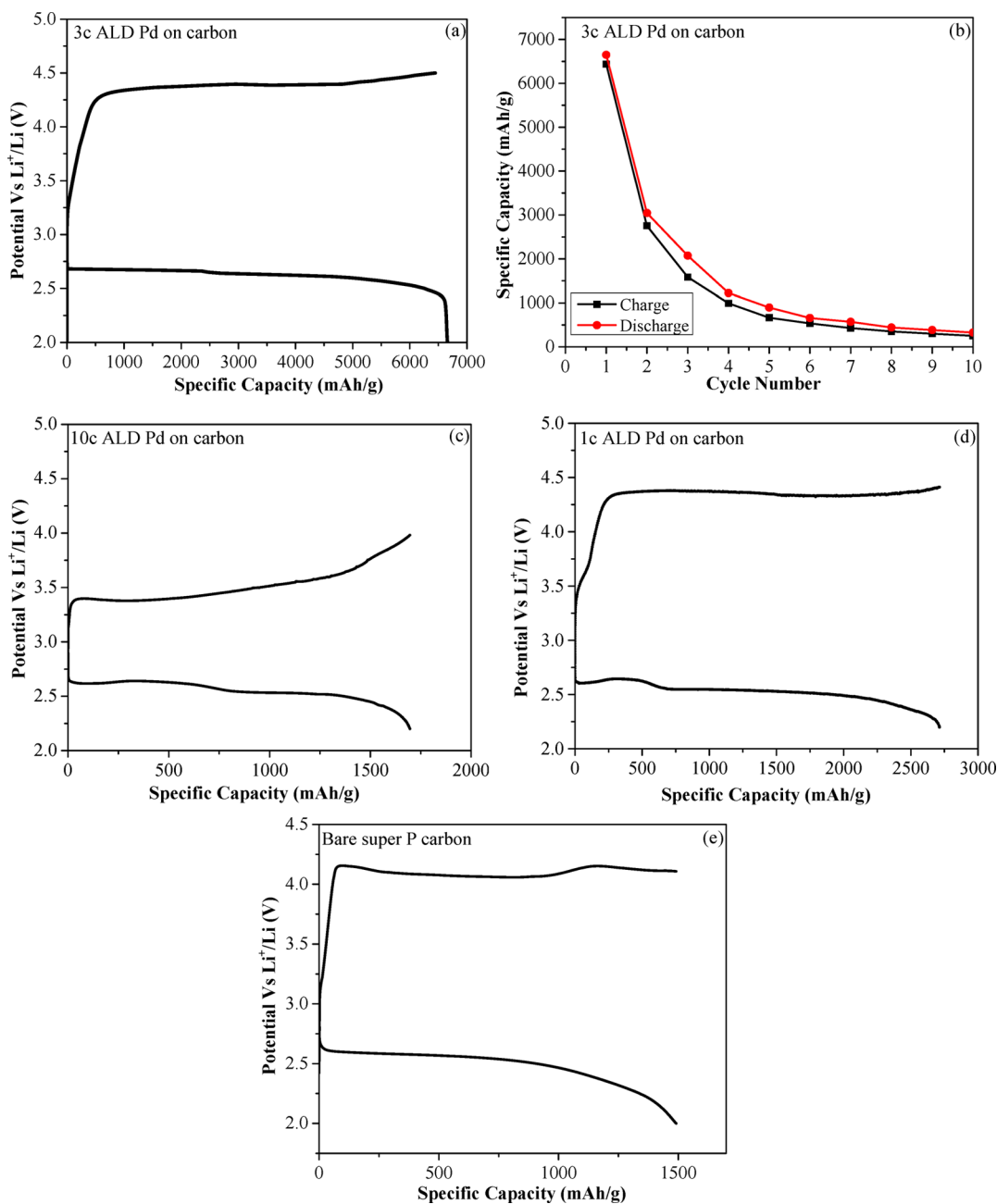
On the basis of all the above results, we conclude the following: (1) the as-prepared Pd/C is surface oxidized and has a crystalline fcc structure, and the average particle size is controlled by the number of ALD Pd cycles to be in the range 2−8 nm; (2) the as-prepared Pd nanoparticles are uniformly distributed on the porous carbon surface. These as-prepared Pd/C composites with porous structures and high specific surface area are of particular interest, since they can provide more active sites to absorb O_2 molecules. This should enhance

the catalytic activity for the oxygen reduction reaction (ORR) and the oxygen evolution reaction (OER), as we demonstrate below for the Li−O_2 cell.

A Swagelok-type cell consisting of a Li-foil anode and an as-prepared 3c-ALD Pd/C cathode was tested under O_2 atmosphere with a MACCOR cycler. TEGDME-LiCF$_3$SO$_3$ was selected as an electrolyte, since it was recently demonstrated to be relatively stable toward the discharge product, Li_2O_2, during the discharge reaction.[52] For comparison, the cell containing the cathode with the same loading of SPL carbon only was also tested under similar conditions. Figure 3a shows voltage profiles of the first discharge to 2.0 V (deep discharge) under a discharge rate of 100 mA/g. The initial discharge reaction of the cell containing the 3c-ALD Pd/C cathode takes place at approximately 2.70 V, with a total specific capacity of about 6600 mAh/g. The cell with only bare SPL carbon as the cathode, however, only delivered about 1500 mAh/g with a discharge voltage of 2.5 V, which is a few hundred millivolts lower than that of the 3c-ALD Pd/C cathode. This finding provides strong evidence that the oxygen reduction reaction during discharge in the Li−O_2 cell is greatly facilitated when 3c-ALD Pd on carbon is used as the electrocatalyst, which not only contributes to a higher capacity by providing more active sites for the ORR reaction but also leads to a higher discharge potential. The discharge products on the 3c-ALD Pd/C cathode were subjected to XRD measurement, and results are shown in Figure 3b. The diffraction patterns of the discharged cathode clearly show that Li_2O_2 is the main discharge product on the 3c-ALD Pd/C cathode, while the discharge product on the bare carbon cathode appeared to be only LiOH with no evidence of crystalline Li_2O_2.[53] Note that a small amount of the LiOH was also detected on the 3c-ALD Pd/C samples, which is likely due to the reaction between Li_2O_2 and H_2O either from the residual moisture left on the electrode or from the air during the XRD measurements. The SEM image of the 3c-ALD Pd/C cathode harvested after first discharge clearly showed a large amount of "donut"-like particles, presumably Li_2O_2,[54] filled the pores of the carbon cathode (Supporting Information, Figure S3), while only amorphous-like products are observed for the bare carbon cathode after first discharge (Supporting Information, Figure

Figure 3. (a) Voltage profile of the first discharge for a cathode containing bare carbon and 3c-ALD Pd/C in 1 M LiCF$_3$SO$_3$/TEGDME at 100 mA/g. (b) XRD patterns of a cathode containing 3c-ALD Pd/C (bottom) and 10c-ALD Pd/C (top) as active materials after first discharge to 2.0 and 2.2 V, respectively.

Figure 4. (a) Voltage profile of the first cycle for a cathode containing 3c-ALD Pd in carbon matrix cycling in 1 M LiCF$_3$SO$_3$/TEGDME at 100 mA/g. (b) Cell capacity as a function of cycle number for air electrodes containing 3c-ALD Pd in carbon matrix cycling in 1 M LiCF$_3$SO$_3$/TEGDME at 100 mA/g. (c) Voltage profile of the first cycle for a cathode containing 10c-ALD Pd in carbon matrix cycling in 1 M LiCF$_3$SO$_3$/TEGDME at 100 mA/g. (d) Voltage profile of the first cycle for cathode containing 1c-ALD Pd in carbon matrix cycling in 1 M LiCF$_3$SO$_3$/TEGDME at 100 mA/g. (e) Voltage profile of the first cycle for bare carbon cathode cycling in 1 M LiCF$_3$SO$_3$/TEGDME at 100 mA/g.

S4). This result probably indicates that the nucleation of Li$_2$O$_2$ strongly depends on the catalytic surface.
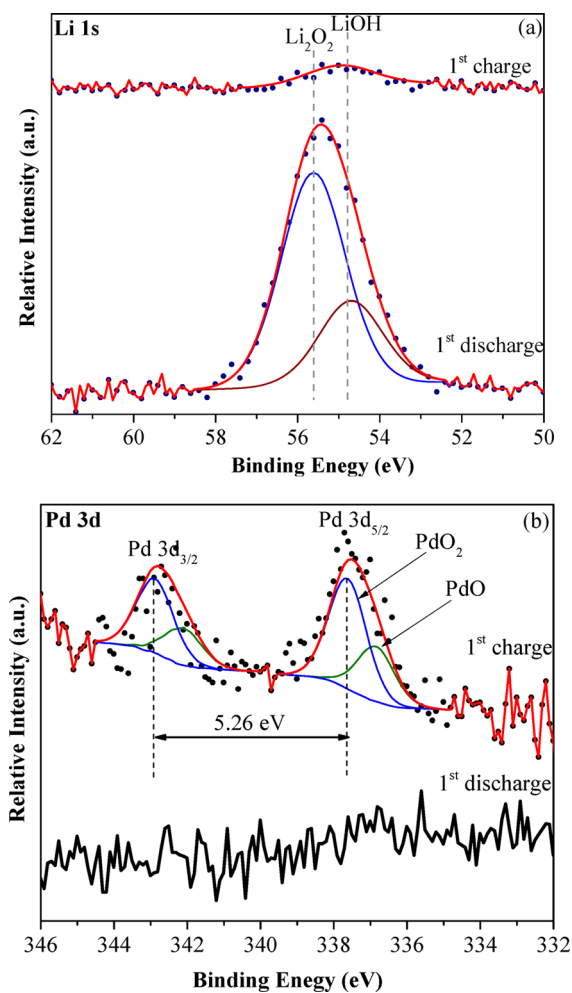
In an attempt to fully recover the discharge product, we employed an equal-capacity charging mode in which the cutoff charging condition was specified so that the charging capacity matched the previous discharging capacity, while the charge potential was limited to 4.5 V. Under this mode, the charge of the cell was terminated when either of these conditions was achieved. Figure 4a shows the cycle performance of the Li−O$_2$ cell containing the 3c-ALD Pd/C cathode, from which it can be seen that severe polarization occurred during the first charge. Around 6500 mAh/g was recovered at the 4.3 V plateau during

the charge, which accounts for more than 98% (Columbic efficiency) of the discharge capacity. On the second discharge to 2.0 V, the capacity dropped dramatically to 3000 mAh/g. This result indicates that part of this capacity recovered during the first cycle may come from the electrolyte decomposition at relatively high charge potential (>4.3 V).[55] In other words, Li$_2$O$_2$ formed during the first discharge does not completely decompose upon charging, which leads to the blocking of the active site or pores. The SEM image of the cathode after being charged on the first cycle (Supporting Information, Figure S5) indeed showed some toroid-like Li$_2$O$_2$ left on the surface, supporting the above clarification. The deep discharge

conditions can also lead to poor cycle performance once an accumulation of the insulating discharge products, particularly lithium peroxide, impedes the transportation of lithium ions, oxygen, and electrons in the electrode. Another possible cause of capacity failure is the poisoning of the Pd catalyst by contaminants or passivation. A buildup of contaminants such as Li_2CO_3 could be the result of gradual decomposition of the TEGDME electrolyte such as by reaction with the Li_2O_2 surface, as found experimentally.[56] All of these aspects would likely lead to the poor cycle performance of the Li−O$_2$ cell, as presented above.

Figure 4c illustrates the voltage profile of the first cycle for the 10c-ALD Pd sample as the cathode material in a Li−O$_2$ cell. A similar discharge potential (∼2.7 V) was achieved which shows the catalytic effect of the 10c-ALD Pd sample toward the oxygen reduction reaction during discharge in the Li−O$_2$ cell, although the cell delivers much less capacity (∼1700 mAh/g) compared to the 3c-ALD Pd sample. The decrease of the capacity of the 10c-ALD sample compared with the 3c-ALD sample is probably due to the loss of the active site on the cathode surface. The discharge products on the 10c-ALD Pd cathode mainly consist of Li_2O_2, as shown in Figure 3b. Surprisingly, the charge potential is significantly lowered to about ∼3.4 V, compared to that of 3c-ALD Pd (Figure 4b), 1c-ALD Pd (Figure 4d), and bare carbon (Figure 4e) samples, and this charge potential can be maintained for several cycles (>5). At this stage, we do not completely understand the mechanism that leads to the low charge overpotential for the 10c-ALD Pd sample, which needs to be further explored. It is likely that more coverage of the carbon surface (i.e., the defect sites) in the 10c-ALD Pd sample would not only lead to better electron transfer for the nucleation and growth of Li_2O_2 but also would minimize the possible electrolyte decomposition on the carbon defect sites. Such electrolyte decomposition will result in the deposition of contaminants such as carbonates on the lithium peroxide or on the carbon surface and would likely increase the charge potential. Nevertheless, this is an encouraging result showing that a low charge potential can be achieved when a suitable electrocatalyst is applied to the carbon. It should also be noted that there appear to be two discharge plateaus during the discharge of all ALD-Pd coated carbon samples, which is likely attributed to the impedance change due to the insulation nature of the discharge product, Li_2O_2.

X-ray photoelectron spectra (XPS) was used to investigate the catalyst surface and identify the discharge and charge products during the electrochemical reactions, which were obtained from the 10c-ALD Pd/C cathode in the first discharged and first charged state, respectively. The Li 1s and Pd 3d XPS spectra were recorded and fitted, as shown in Figure 5. Figure 5a (bottom spectrum) shows the Li 1s XPS spectrum for the first discharge sample, from which it can be concluded that lithium peroxide formed as the dominated discharge product of the electrochemical reactions[53] along with a small amount of LiOH, which is consistent with the XRD results. The XPS data confirm that the desired discharge product (lithium peroxide) can be produced when a suitable catalyst, in this case the 10c-ALD Pd/C composite, is introduced on the cathode. On the basis of the above XRD and XPS results, it is clearly demonstrated that the catalyst plays a key role in facilitating the oxygen reduction reaction and forming the desired discharge product, Li_2O_2. Upon charging, the lithium signals from lithium peroxide completely disappeared (Figure 5a, first charge), suggesting that these discharged products decompose during

Figure 5. XPS spectra of (a) Li 1s and (b) Pd 3d core peaks of the cathode containing as-prepared 10c-ALD Pd/C at different charge/discharge status.

the charging process. This finding provides solid evidence that lithium peroxide can be formed and decomposed reversibly during the cycle test of the TEGDME-based Li−O$_2$ cells.

Figure 5b presents the Pd 3d core level XPS spectra of the prepared 10c-ALD Pd/C cathode for different electrochemical treatments (charge/discharge), as marked in the figure. Analysis of the Pd 3d spectrum for the first discharge electrode shows no Pd signal, indicating that Li_2O_2 was sufficiently thick to completely attenuate photoelectrons from the Pd nanoparticles. In other words, the oxygen reduction reaction does take place on the surface of the catalyst during discharge of the cell. The Pd signal reappeared in the charged samples (first charge in Figure 5b), since the discharge products were decomposed and removed from the electrode surface. It should also be noted that the Pd nanoparticle surface oxidized to PdO_2 during the cycle testing in the Li−O$_2$ cell.

Finally, it should be noted that, although TEGDME, which is used in the present study as the electrolyte, is suspected to be unstable on deep discharge in Li−O$_2$ cells at potential <2.4 V, it is still of great interest to explore the reactions that may occur in the presence of different catalysts that may promote the two-electron reduction of oxygen to lithium peroxide. Irrespective of the electrolyte problems mentioned above, and in parallel to new efforts with more promising electrolytes,[52,57] our goal in this study has been to explore a novel approach and design new

electrode/electrocatalytic materials for the oxygen cathode, which might help overcome at least some of the limitations of current Li−O$_2$ cells. Needless to say, further in-depth research is required to fully identify the discharge and charge products and understand the effects of electrolytes on the electrochemical performance of the current Li−O$_2$ cells, which will be addressed in future work by the present authors.

In summary, ALD was used to synthesize Pd nanoparticles on a porous carbon support and the resulting materials were employed as electrocatalysts for rechargeable Li−O$_2$ cells. Both XRD and XAS analyses confirmed the presence of crystalline, metallic Pd. The conformal attribute of ALD ensured that the Pd nanoparticles were uniformly dispersed over the high surface area carbon support, and that the porous structure and surface area were well persevered. As a consequence, the as-prepared catalysts demonstrated a superior electrochemical behavior, and delivered a capacity of up to 6600 mAh/g (carbon + electrocatalyst) using a current density of 100 mA/g. This reaction was reasonably reversible during the early cycles. Our results suggest that ALD is a promising technique for tailoring the surface composition and structure of porous supports in energy storage devices.

■ ASSOCIATED CONTENT

Ⓢ Supporting Information
Experimental details, SEM images for the sample before and after the ALD Pd process, and SEM images of the bare carbon and 3c-ALD Pd/C cathode harvested after first discharge and first charge. This material is available free of charge via the Internet at http://pubs.acs.org.

■ AUTHOR INFORMATION

Corresponding Author
*E-mail: amine@anl.gov (K.A.); jelam@anl.gov (J.W.E.). Phone: 1-630-252-3838 (K.A.); 1-630-252-3520 (J.W.E.).

Author Contributions
∇These authors contributed equally.

Notes
The authors declare no competing financial interest.

■ ACKNOWLEDGMENTS

■ REFERENCES

(1) Abraham, K. M.; Jiang, Z. *J. Electrochem. Soc.* **1996**, *143*, 1.
(2) Ogasawara, T.; Debart, A.; Holzapfel, M.; Novak, P.; Bruce, P. G. *J. Am. Chem. Soc.* **2006**, *128*, 1390.
(3) Jiao, F.; Bruce, P. G. *Adv. Mater.* **2007**, *19*, 657.
(4) Debart, A.; Paterson, A. J.; Bao, J.; Bruce, P. G. *Angew. Chem., Int. Ed.* **2008**, *47*, 4521.
(5) Laoire, C. O.; Mukerjee, S.; Abraham, K. M.; Plichta, E. J.; Hendrickson, M. A. *J. Phys. Chem. C* **2009**, *113*, 20127.
(6) Williford, R. E.; Zhang, J.-G. *J. Power Sources* **2009**, *194*, 1164.
(7) Andrei, P.; Zheng, J. P.; Hendrickson, M.; Plichta, E. J. *J. Electrochem. Soc.* **2010**, *157*, A1287.
(8) Deyu, W.; Jie, X.; Wu, X.; Ji-Guang, Z. *J. Electrochem. Soc.* **2010**, *157*.
(9) Eswaran, M.; Munichandraiah, N.; Scanlon, L. G. *Electrochem. Solid-State Lett.* **2010**, *13*, A121.
(10) Girishkumar, G.; McCloskey, B.; Luntz, A. C.; Swanson, S.; Wilcke, W. *J. Phys. Chem. Lett.* **2010**, *1*, 2193.
(11) Hummelshoj, J. S.; Blomqvist, J.; Datta, S.; Vegge, T.; Rossmeisl, J.; Thygesen, K. S.; Luntz, A. C.; Jacobsen, K. W.; Norskov, J. K. *J. Chem. Phys.* **2010**, *132*.
(12) Jian, Z.; Wu, X.; Xiaohong, L.; Wei, L. *J. Electrochem. Soc.* **2010**, *157*.
(13) Jie, X.; Donghai, W.; Wu, X.; Deyu, W.; Williford, R. E.; Jun, L.; Ji-Guang, Z. *J. Electrochem. Soc.* **2010**, *157*.
(14) Lu, Y.-C.; Gasteiger, H. A.; Crumlin, E.; McGuire, R., Jr.; Shao-Horn, Y. *J. Electrochem. Soc.* **2010**, *157*, A1016.
(15) Lu, Y.-C.; Gasteiger, H. A.; Parent, M. C.; Chiloyan, V.; Shao-Horn, Y. *Electrochem. Solid-State Lett.* **2010**, *13*, A69.
(16) Lu, Y.-C.; Xu, Z.; Gasteiger, H. A.; Chen, S.; Hamad-Schifferli, K.; Shao-Horn, Y. *J. Am. Chem. Soc.* **2010**, *132*, 12170.
(17) Thapa, A. K.; Saimen, K.; Ishihara, T. *Electrochem. Solid-State Lett.* **2010**, *13*, A165.
(18) Bruce, P. G.; Hardwick, L. J.; Abraham, K. M. *MRS Bull.* **2011**, *36*, 506.
(19) Trahey, L.; Johnson, C. S.; Vaughey, J. T.; Kang, S. H.; Hardwick, L. J.; Freunberger, S. A.; Bruce, P. G.; Thackeray, M. M. *Electrochem. Solid-State Lett.* **2011**, *14*, A64.
(20) Wang, Y.; Zhou, H. *Energy Environ. Sci.* **2011**, *4*, 1704.
(21) Xu, W.; Xu, K.; Viswanathan, V. V.; Towne, S. A.; Hardy, J. S.; Xiao, J.; Hu, D.; Wang, D.; Zhang, J.-G. *J. Power Sources* **2011**, *196*, 9631.
(22) Yoo, E.; Zhou, H. *ACS Nano* **2011**, *5*, 3020.
(23) Freunberger, S. A.; Chen, Y.; Drewett, N. E.; Hardwick, L. J.; Barde, F.; Bruce, P. G. *Angew. Chem., Int. Ed.* **2011**, *50*, 8609.
(24) Freunberger, S. A.; Chen, Y.; Peng, Z.; Griffin, J. M.; Hardwick, L. J.; Barde, F.; Novak, P.; Bruce, P. G. *J. Am. Chem. Soc.* **2011**, *133*, 8040.
(25) McCloskey, B. D.; Bethune, D. S.; Shelby, R. M.; Girishkumar, G.; Luntz, A. C. *J. Phys. Chem. Lett.* **2011**, *2*, 1161.
(26) Kuboki, T.; Okuyama, T.; Ohsaki, T.; Takami, N. *J. Power Sources* **2005**, *146*, 766.
(27) Qin, Y.; Lu, J.; Du, P.; Chen, Z.; Ren, Y.; Wu, T.; Miller, J. T.; Wen, J.; Miller, D. J.; Zhang, Z.; Amine, K. *Energy Environ. Sci.* **2013**, *6*, 519.
(28) Zhang, G. Q.; Zheng, J. P.; Liang, R.; Zhang, C.; Wang, B.; Au, M.; Hendrickson, M.; Plichta, E. J. *J. Electrochem. Soc.* **2011**, *158*, A822.
(29) Ren, X.; Zhang, S. S.; Tran, D. T.; Read, J. *J. Mater. Chem.* **2011**, *21*, 10118.
(30) Lu, Y.-C.; Gasteiger, H. A.; Shao-Horn, Y. *Electrochem. Solid-State Lett.* **2011**, *14*, A70.

(31) Ku-Bong, C.; Ju-Kyung, S.; Tae-Young, J.; Dong-Kyun, N.; Yongsug, T.; Sung-Hyeon, B. *Rev. Adv. Mater. Sci.* **2011**, *28*.

(32) Chen, J.; Hummelshoj, J. S.; Thygesen, K. S.; Myrdal, J. S. G.; Norskov, J. K.; Vegge, T. *Catal. Today* **2011**, *165*, 2.

(33) Xu, W.; Xiao, J.; Wang, D. Y.; Zhang, J.; Zhang, J. G. *J. Electrochem. Soc.* **2010**, *157*, A219.

(34) Puurunen, R. L. *J. Appl. Phys.* **2005**, *97*, 121301.

(35) Leskela, M.; Ritala, M. *Thin Solid Films* **2002**, *409*, 138.

(36) Elam, J. W.; Routkevitch, D.; Mardilovich, P. P.; George, S. M. *Chem. Mater.* **2003**, *15*, 3507.

(37) Shin, H. J.; Jeong, D. K.; Lee, J. G.; Sung, M. M.; Kim, J. Y. *Adv. Mater.* **2004**, *16*, 1197.

(38) Chen, P.; Mitsui, T.; Farmer, D. B.; Golovchenko, J.; Gordon, R. G.; Branton, D. *Nano Lett.* **2004**, *4*, 1333.

(39) Pellin, M. J.; Stair, P. C.; Xiong, G.; Elam, J. W.; Birrell, J.; Curtiss, L.; George, S. M.; Han, C. Y.; Iton, L.; Kung, H.; Kung, M.; Wang, H. H. *Catal. Lett.* **2005**, *102*, 127.

(40) Jiang, X. R.; Huang, H.; Prinz, F. B.; Bent, S. F. *Chem. Mater.* **2008**, *20*, 3897.

(41) Herrera, J. E.; Kwak, J. H.; Hu, J. Z.; Wang, Y.; Peden, C. H. F.; Macht, J.; Iglesia, E. *J. Catal.* **2006**, *239*, 200.

(42) Keranen, J.; Auroux, A.; Ek, S.; Niinisto, L. *Appl. Catal., A* **2002**, *228*, 213.

(43) Lei, Y.; Mehmood, F.; Lee, S.; Greeley, J.; Lee, B.; Seifert, S.; Winans, R. E.; Elam, J. W.; Meyer, R. J.; Redfern, P. C.; Teschner, D.; Schlogl, R.; Pellin, M. J.; Curtiss, L. A.; Vajda, S. *Science* **2010**, *328*, 224.

(44) Feng, H.; Libera, J. A.; Stair, P. C.; Miller, J. T.; Elam, J. W. *ACS Catal.* **2011**, *1*, 665.

(45) Lu, J. L.; Stair, P. C. *Angew. Chem., Int. Ed.* **2010**, *49*, 2547.

(46) Christensen, S. T.; Elam, J. W.; Rabuffetti, F. A.; Ma, Q.; Weigand, S. J.; Lee, B.; Seifert, S.; Stair, P. C.; Poeppelmeier, K. R.; Hersam, M. C.; Bedzyk, M. J. *Small* **2009**, *5*, 750.

(47) Lei, Y.; Lu, J.; Zhao, H. Y.; Liu, B.; Low, K.-B.; Wu, T. P.; Libera, J. A.; Greeley, J. P.; Chupas, P. J.; Miller, J. T.; Elam, J. W. *J. Phys. Chem. C* **2013**, *117*, 11141.

(48) Feng, H.; Elam, J. W.; Libera, J. A.; Setthapun, W.; Stair, P. C. *Chem. Mater.* **2010**, *22*, 3133.

(49) Lu, J. L.; Fu, B. S.; Kung, M. C.; Xiao, G. M.; Elam, J. W.; Kung, H. H.; Stair, P. C. *Science* **2012**, *335*, 1205.

(50) Lu, J. L.; Stair, P. C. *Langmuir* **2010**, *26*, 16486.

(51) Shao, M. H.; Yu, T.; Odell, J. H.; Jin, M. S.; Xia, Y. N. *Chem. Commun.* **2011**, *47*, 6566.

(52) Laoire, C. O.; Mukerjee, S.; Plichta, E. J.; Hendrickson, M. A.; Abraham, K. M. *J. Electrochem. Soc.* **2011**, *158*, A302.

(53) Lu, J.; Qin, Y.; Du, P.; Luo, X.; Wu, T.; Ren, Y.; Wen, J.; Miller, D. J.; Miller, J. T.; Amine, K. *RSC Adv.* **2013**, *3*, 8276.

(54) Lu, Y.-C.; K., D. G.; Yao, K. P. C.; Harding, J. R.; Zhou, J.; Zuin, L.; Yang, S.-H. *Energy Environ. Sci.* **2011**, *4*, 2999.

(55) McCloskey, B. D.; Scheffler, R.; Speidel, A.; Girishkumar, G.; Luntz, A. C. *J. Phys. Chem. C* **2012**, *116*, 23897.

(56) McCloskey, B. D.; Speidel, A.; Scheffler, R.; Miller, D. C.; Viswanathan, V.; Hummelshoj, J. S.; Norskov, J. K.; Luntz, A. C. *J. Phys. Chem. Lett.* **2012**, *3*, 997.

(57) Zhang, Z. C.; Lu, J.; Assary, R. S.; Du, P.; Wang, H. H.; Sun, Y. K.; Qin, Y.; Lau, K. C.; Greeley, J.; Redfern, P. C.; Iddir, H.; Curtiss, L. A.; Amine, K. *J. Phys. Chem. C* **2011**, *115*, 25535.